

l_1 -ball Prior: Uncertainty Quantification with Exact Zeros

Maoran Xu ^{*} Leo L. Duan [†]

November 9, 2021

Abstract: Lasso and l_1 -regularization play a dominating role in high dimensional statistics and machine learning. The most attractive property is that it produces a sparse parameter estimate containing exact zeros. For uncertainty quantification, popular Bayesian approaches choose a continuous prior that puts concentrated mass near zero; however, as a limitation, the continuous posterior cannot be exactly sparse. This makes such a prior problematic for advanced models, such as the change-point detection, linear trend filtering and convex clustering, where zeros are crucial for dimension reduction. In this article, we propose a new class of prior, by projecting a continuous distribution onto the l_1 -ball with radius r . This projection creates a positive probability on the lower-dimensional boundary of the ball, where the random variable now contains both continuous elements and exact zeros; meanwhile, assigning prior for radius r gives robustness to large signals. Compared with the spike-and-slab prior, our proposal has substantial flexibility in the prior specification and adaptive shrinkage on small signals; in addition, it enjoys an efficient optimization-based posterior estimation. In asymptotic theory, the prior attains the minimax optimal rate for the posterior concentration around the truth; in practice, it enables a direct application of the rich class of l_1 -tricks in Bayesian models. We demonstrate its potentials in a data application of analyzing electroencephalogram time series data in human working memory study, using a non-parametric mixture model of linear trend filters.

KEY WORDS: Cardinality, Data Augmentation, Reversified Projection, Thresholding, Transport Monte Carlo.

^{*}Department of Statistics, University of Florida, U.S.A. maoranxu@ufl.edu

[†]Department of Statistics, University of Florida, U.S.A. li.duan@ufl.edu

1 Introduction

The l_1 -regularization has been a milestone in high dimensional statistics and machine learning. Since its introduction in Lasso regression for solving variable selection problem [Tibshirani, 1996], it has inspired a rich class of algorithms and models—an incomplete list of representative works cover areas of regression [Efron et al., 2004, Zou and Hastie, 2005, Yuan and Lin, 2006], multivariate data analysis [Chen et al., 2001, Zou et al., 2006], graph estimation [Shojaie and Michailidis, 2010, Zhang and Zou, 2014, Fan et al., 2017], among others. For comprehensive reviews, see Meinshausen and Bühlmann [2006], and more recently Bühlmann and Van De Geer [2011].

One of the most appealing properties of l_1 -regularization is that it induces exact zeros in the optimal solution. This is due to the well-known dual form of the l_1 -norm penalty, as equivalent to constraining the parameter on an l_1 -ball centered at the origin. Because of the “spikiness” of the l_1 -ball in high dimension, it makes it possible for a sparse recovery of the signals [See Vershynin [2018] for a formal exposition].

In recent years, it has been demonstrated that the sparse property can be exploited beyond the simple tasks of variable selection. In particular, it can be used to build equivalence (or relaxation) to some complicated combinatorial problems, using the l_1 -tricks—an “over-parameterize and sparsify” modeling strategy that bypasses the difficulty in the cardinality-constrained problems. To give a few concrete examples, in the change-point detection of time series data, the fused lasso [Tibshirani et al., 2005] equips each time point with its own mean, then makes the temporal increment/decrement sparse, effectively creating a step function that captures any abrupt temporal changes. For a clustering problem, the convex clustering [Lindsten et al., 2011, Tan and Witten, 2015] assigns a location parameter to every data point, then tries to sparsify the pairwise distances, leading to only a few unique locations as the cluster centers. In low-rank matrix factorization, one uses an unconstrained matrix as the factor, then regularizes its nuclear norm [Grave et al., 2011] via sparsifying the singular values, effectively achieving a rank reduction. These are just a few examples of the l_1 -tricks; nevertheless, it is clear that the exact zeros are crucial for those methods to work.

In parallel to the development of the above advanced models (mostly in the optimization literature), there has been a booming literature in Bayesian shrinkage priors. These works are largely motivated to address the uncertainty quantification problems, for example: (i) how likely a parameter element is zero vs. non-zero? (ii) how much correlation there is between the non-zero elements? Among the early works, the most well-known is

the Bayesian lasso, which exponentiates the negative l_1 -norm in a double exponential prior [Park and Casella, 2008]; however, it was discovered that except for the posterior mode, the Bayesian lasso deviates considerably from the goal of shrinking redundant elements: there is very little concentration near zero, while the thin tails cause an under-estimation of the non-zero signal. As a result, the posterior distribution from the Bayesian lasso is unable to provide an answer to (i). To address these issues, a rich class of new continuous shrinkage priors have been proposed, where the prior has a large concentration in a neighborhood near zero and heavy tail to accommodate large signals. Examples include the horseshoe [Carvalho et al., 2010], generalized double Pareto [Armagan et al., 2013], Dirichlet-Laplace [Bhattacharya et al., 2015], spike-and-slab lasso [Ročková, Veronika and George, Edward I], Beta-prime [Bai and Ghosh, 2019], among others. Thanks to the efficient computation of the Markov chain Monte Carlo in continuous parameter space, these approaches have become especially popular in high-dimensional Bayesian regression. Nevertheless, as a limitation, the continuous posterior cannot be *exactly sparse* (since the probability is zero for a continuous element to equal to zero), which is problematic to use in the above new models depending on the l_1 -tricks.

As a remedy, one may choose a small threshold to post-process those small elements into zeros. While this may work in simple tasks such as variable selection, such a heuristic can lead to a major sensitivity problem for advanced models—as shown later in our example, for the change point detection, thresholding fails to provide a realistic estimate on the confidence band, while generating sensitivity issues. In addition, the lack of sparse posterior also creates challenges in theoretic analysis, for example, the posterior convergence rate of the model selection will need involve a threshold as well [see Bhattacharya et al. [2015] for a discussion on compressibility].

To fundamentally address this issue, we need a prior that puts positive probability on sets of sparse vector. To our best knowledge, the spike-and-slab prior, formed by the two-component mixture of a point mass at zero (spike) and a continuous distribution (slab) [Lempers, 1971, Mitchell and Beauchamp, 1988] is the only one having this property; yet, it suffers from two major issues: (i) the computational inefficiency due to the combinatorial search, which is the primary reason that motivated the continuous non-sparse approximation [George and McCulloch, 1995, Ishwaran and Rao, 2005] (in addition the continuous priors listed above); (ii) the small signals can confound the noise, as shown later, leading to an over-estimated variance around those zero elements. The source of these issues is that, roughly speaking, it is a rather crude treatment to use the same probability to con-

trol each element to be zero or not. There is a lack of adaptiveness to the individual magnitude of each signal.

Motivated to develop a prior capable of inducing exact sparsity in posterior, while avoiding the caveats of the spike-and-slab prior, we develop a new strategy: starting from a continuous random variable with unconstrained support, we project it onto the l_1 -ball. Since the boundary of the l_1 -ball contains sets of points that are sparse, and any point outside the ball will be projected onto the boundary, we create a positive probability for the random variable to contain exact zeros. The projection is straightforward to compute, and the prior kernel can be obtained in simple form using data augmentation, which is amenable to both Gibbs sampler and fast optimization-based posterior estimation. This prior is theoretically justified and enjoys a minimax optimal rate for posterior convergence towards the true parameter. We will demonstrate competitive performance in various simulations and data applications.

2 l_1 -ball Prior

In this section, we first demonstrate how a simple l_1 -ball projection produces a prior distribution with positive probability for exact sparsity. Then we use the data augmentation technique to “reversify” the projection, and derive a simple probability kernel for this prior.

2.1 Projection to an l_1 -ball

Starting with a parameter space \mathbb{R}^p , our region of interest is on the l_1 ball with radius r and closed boundary,

$$\mathbb{B}_r = \{x \in [-r, r]^p : \|x\|_1 \leq r\},$$

for a given $r > 0$. We denote the interior set by $\mathbf{int} \mathbb{B}_r = \{x \in (-r, r)^p : \|x\|_1 < r\}$, and boundary set by $\mathbf{bd} \mathbb{B}_r = \{x : \|x\|_1 = r\}$.

For any point $\beta \in \mathbb{R}^p$, we can project it onto the l_1 -ball, by solving the following optimization problem,

$$\theta = P_{\mathbb{B}_r}(\beta) = \arg \min_{\|x\|_1 \leq r} \|\beta - x\|_2^2.$$

This problem is strictly convex—that is, for every β , there is only one optimal solution $\theta = P_{\mathbb{B}_r}(\beta)$ (i.e., the mapping is measurable). Here we present

a simple solution [modifying from Duchi et al. [2008]]. If $\|\beta\|_1 > r$,

$$\begin{aligned} \text{Sort } \beta \text{ so that } |\beta_{(1)}| \geq \dots \geq |\beta_{(p)}|, \\ c := \max\{j : |\beta_{(j)}| > \frac{\mu_j}{j}, \mu_j = (\sum_{i=1}^j |\beta_{(i)}| - r)_+\}, \quad (1) \\ \theta_i := \text{sign}(\beta_i) \max(|\beta_i| - \frac{\mu_c}{c}, 0); \end{aligned}$$

where $(x)_+ = x$ if $x > 0$, or $(x)_+ = 0$ if $x \leq 0$. And we let $\theta := \beta$ if $\|\beta\|_1 \leq r$.

Suppose now $\beta \in \mathbb{R}^p$ is a continuous random variable [in a probability space $(\mathbb{R}^p, \mathcal{B}(\mathbb{R}^p), \nu)$, with ν its Lebesgue measure on \mathbb{R}^p] and π_β the associated density. We can compute the probability measure for θ :

$$\text{pr}(\theta \in \mathcal{A}) = \int_{\mathbb{R}^p} \mathbb{I}[P_{\mathbb{B}_r}(x) \in \mathcal{A}] \pi_\beta(x) dx, \quad (2)$$

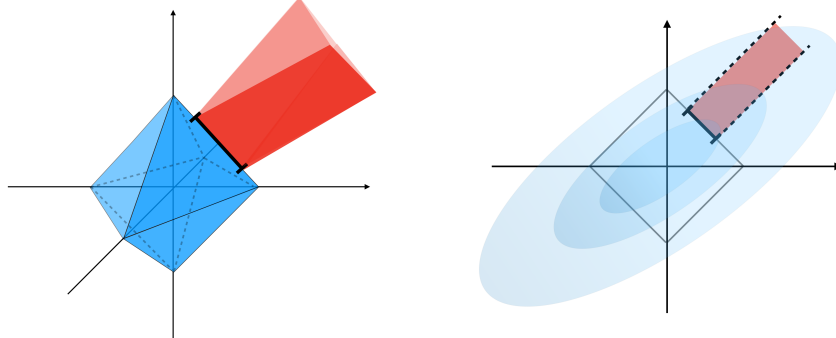
where $\mathbb{I}(E) = 1$ if event E is true, otherwise takes value 0, \mathcal{A} is a set in \mathbb{B}_r .

Combining (1) and (2), we note two important results:

1. If $c < p$, there will be $(p - c)$ elements of $\theta_i = 0$; hence exact sparsity happens on the boundary $\mathbf{bd} \mathbb{B}_r$.
2. All the points outside the ball $\beta \in \mathbb{R}^p \setminus \mathbb{B}_r$ will be projected to $\theta \in \mathbf{bd} \mathbb{B}_r$, therefore, the boundary set has a positive probability.

These results inspire us to consider a simple way to develop exactly sparse priors $\pi_0(\theta)$ (i.e., having *positive* probability for some element $\theta_i = 0$): assigning a continuous prior on β and projecting it onto \mathbb{B}_r .

To illustrate the geometric intuition, we show the projection in \mathbb{R}^3 [Figure 1]—projecting β from a multivariate Gaussian to $\theta \in \mathbb{B}_r$ gives us positive probability $\text{pr}[\theta = (x_1, 0, x_3)] > 0$, which is equal to the Gaussian measure in the wedge region outside \mathbb{B}_r . This would be impossible if θ were assigned a continuous prior in \mathbb{R}^p , since fixing any $\theta_i = 0$ would cause the probability to collapse to zero.



(a) All the points β in the red area are projected to θ in the line segment $\{(x, 0, r - x) : 0.2 < x < 0.8\}$, which contains exact zero $\theta_2 = 0$.

(b) Sectional view in 2-dimensions: the probability of θ in the line segment is equal to the measure of β over the area in the red, which is positive.

Figure 1: Projecting a continuous Gaussian $\beta \in \mathbb{R}^3$ to θ onto an l_1 -ball \mathbb{B}_r (the right panel shows a density contour in 2-dimensions): the boundary set of θ containing exactly zero has a positive probability. For example, the probability of θ in the line segment $\{(x, 0, r - x) : 0.2 < x < 0.8\}$ is equal to the probability of β over the red region.

Using this intuition, we can now formally derive the prior of θ . This can be obtained in a simple closed-form with data augmentation.

2.2 Deriving Closed-form Prior via Data Augmentation

The first thing to note is that when $\theta \in \text{bd } \mathbb{B}_r$, the elements of θ contain both zeros and continuous random variables. Therefore, we associate θ with a prior *kernel* $\pi_0(\theta)$, a function $\pi_0 : \mathbb{B}_r \rightarrow [0, \infty)$, as the mix of probability mass and density functions, which should be integrable to 1 over \mathbb{B}_r .

Let $[p] = \{1, \dots, p\}$ be the full element indices, and $C = \{i \in [p] : \theta_i \neq 0\}$ a subset for those non-zero elements with $c := |C|$. And we use subscript to denote the non-zero sub-vector $\theta_C = (\theta_i)_{i \in C}$. We now divide the l_1 -ball projection into two steps: (i) one-to-one transform of β into a set of latent variables; (ii) integrating over those falling below zero, corresponding to zero-thresholding.

In step (i), consider latent variables $t = (t_1, \dots, t_p)$, $s = (s_1, \dots, s_p)$ and

μ , defined as

$$t_i = |\beta_i| - \frac{\mu}{c}, \quad s_i = \text{sign}(\beta_i),$$

$$\mu = \mu_c, \quad c = \max\{j : |\beta_{(j)}| > \frac{\mu_j}{j}\}, \quad \mu_j = (\sum_{i=1}^j |\beta_{(i)}| - r)_+.$$

As proven later in the theory section, the transform between β and (t, s, μ) is one-to-one hence reversible, despite the sorting in $\beta_{(j)}$. Denoting it by $(t, s, \mu) = f(\beta)$, we can now derive the kernel for (t, s, μ) .

Theorem 1. *With $(t, s, \mu) = f(\beta)$ defined as above, for any proper density π_β ,*

$$\pi_{t,s,\mu}[f(\beta)] = \pi_\beta(\beta)|J_f|,$$

where $|J_f|$ is the absolute determinant of the Jacobian, and $|J_f| = 1$. Equivalently, $\pi_0(t, s, \mu) = \pi_\beta[f^{-1}(t, s, \mu)]$.

Remark 1. *The constant $|J_f| = 1$ shows that f is a volume-preserving transform, hence the derived kernel is invariant to the number of non-zeros in θ , simplifying the posterior computation.*

In step (ii), we obtain a sparse θ via the signed zero-thresholding $\theta_i = s_i(t_i)_+$. Equivalently, we can view $\pi_0(\theta)$ as the marginal form for $\pi_0(t, s, \mu)$, marginalized over those $t_i < 0$, their signs s_i and the extra parameter $\mu > 0$:

$$\begin{aligned} \pi_0(\theta) &= \pi_0(\theta_i = s_i t_i \text{ for } i \in C; \theta_i = 0 \text{ for } i \notin C) \\ &= \sum_{s_i = \pm 1 \text{ for } i \notin C} \int_0^\infty \int_{(-\mu/c, 0)^{p-c}} \pi_0(t, s, \mu) dt_{[p] \setminus C} d\mu. \end{aligned}$$

In general, the above marginalization may not be tractable, however, we do have closed-form on the augmented $\pi_0(t, s, \mu)$, thanks to Theorem 1.

Therefore, we can use the data augmentation Monte Carlo [Tanner and Wong, 1987] for posterior estimation—specifically, let $L(y; \theta, \eta)$ be the likelihood, y the data, η some other parameter with prior $\pi_0(\eta)$, we can sample the posterior of (t, s, μ) and η via:

$$\begin{aligned} \pi(t, s, \mu, \eta \mid y) &\propto \pi_0(\eta) \pi_0(t, s, \mu) L[y; \theta, \eta : \theta_i = s_i(t_i)_+] \\ &= \pi_0(\eta) \pi_\beta(\beta) L[y; P_{\mathbb{B}_r}(\beta), \eta] \end{aligned} \tag{3}$$

After obtaining the posterior sample of η and $\theta = P_{\mathbb{B}_r}(\beta)$, we discard the other information in (t, s, μ) . We provide the details of the sampling algorithm in the computation section.

For a clear exposition, we will focus on independent double-exponential $\beta_i \sim \text{DE}(0, \lambda_i)$, $\pi(\beta_i) = 1/(2\lambda_i) \exp(-|\beta_i|/\lambda_i)$, with $\lambda_i > 0$. We choose this form for its ease of integration in the theoretic analysis. One can freely choose other continuous $\pi_\beta(\beta)$ such as multivariate Gaussian.

Transforming β to (t, s, μ) , we obtain the prior kernel

$$\pi_0(t, s, \mu) = \prod_{i=1}^p \frac{1}{2\lambda_i} \exp\left(-\frac{\mu/c}{\lambda_i}\right) \exp\left(-\frac{t_i}{\lambda_i}\right),$$

subject to constraints $t_i > -\mu/c$ and $\sum_{i=1}^p (t_i)_+ = r$.

2.3 Prior on the Radius via the Random Threshold

Thus far, we have viewed $r = \|\theta\|_1$ (the radius of \mathbb{B}_r) as given. As we do not know r as a priori, we will treat it as a unknown parameter, assign a prior and estimate it from the posterior.

In order to choose a sensible prior, we get inspiration from the use of soft-thresholding operator in lasso [Tibshirani, 1996]. We make a similar connection here: given a random threshold $\tilde{\mu} = \mu/c$ as in (1), r is completely determined by $\tilde{\mu}$ and β : $r = \sum_{i=1}^p (|\beta_i| - \tilde{\mu})_+$.

Therefore, a choice on $\pi_0(\tilde{\mu})$ is a choice on $\pi_0(r)$. Further, $\tilde{\mu}$ enjoys a very intuitive interpretation—a random threshold that changes a continuous distribution $\pi_\beta(\beta)$ into a sparse $\pi_0(\theta)$. As shown in Figure 2, $\tilde{\mu}$ divides the distribution $\pi(|\beta|)$ into two parts, corresponding to $|\beta_i| \leq \tilde{\mu}$ associated with the point mass $\theta_i = 0$, and $|\beta_i| > \tilde{\mu}$ associated with $|\theta_i| > 0$.

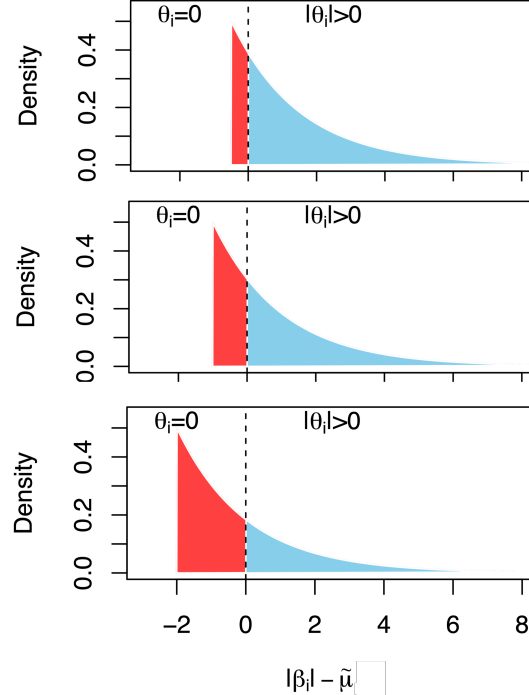


Figure 2: A random-thresholding view of the l_1 -ball prior, when the radius r is treated as a free parameter—this is equivalent to having a free threshold parameter $\tilde{\mu}$, which divides the distribution $\pi(|\beta|)$ into two parts, corresponding to $|\beta_i| \leq \tilde{\mu}$ and $\theta_i = 0$ (red), or $|\beta_i| > \tilde{\mu}$ and $|\theta_i| > 0$ (blue).

Using double-exponential β_i , we can marginalize over those $t_i < 0$, obtaining

$$\begin{aligned} \text{pr}(\theta_i = 0) &= 1 - \exp\left(-\frac{\tilde{\mu}}{\lambda_i}\right), & \text{pr}(|\theta_i| > 0) &= \exp\left(-\frac{\tilde{\mu}}{\lambda_i}\right), \\ \pi_0(\theta \mid |\theta_i| > 0) &= \frac{1}{2\lambda_i} \exp\left(-\frac{|\theta_i|}{\lambda_i}\right). \end{aligned} \tag{4}$$

To assign a prior on $\tilde{\mu}$, we can first assign a hyper-prior for $\lambda_i \sim \text{Inverse-Gamma}(a, b)$. After marginalizing out λ_i , we obtain $\pi(\beta_i \mid a, b) \propto (1 + |\beta_i|/b)^{-(a+1)}$, with $\text{pr}(|\beta_i| \leq x) = 1 - (1 + x/b)^{-a}$, as equivalent to generalized double Pareto distribution [Armagan et al., 2013].

Therefore, if we are to impose a prior belief that $\text{pr}(\theta_i = 0) = 1 - w$, we can choose $\tilde{\mu}$ to be the $(1 - w)$ -quantile, equal to $(w^{-1/a} - 1)b$, with

$w \in (0, 1)$ selected as a priori, or from a certain prior distribution such as $\text{Beta}(1, b_w)$.

Remark 2. Note that if we force all λ_i 's to be the same, then (4) would be a spike-and-slab prior with double exponential slab [Castillo et al., 2015]. However, a major difference in using the individual λ_i and a common threshold is that —now the “spike” probability changes with the scale of the “slab”: as $\lambda_i \rightarrow 0$, $\text{pr}(\theta_i = 0) \rightarrow 1$. Therefore, this gives an adaptiveness that increases the chance for shrinking small noise to zero, while decreases the chance of removing large signals. We will show a clear difference in the data experiments.

3 Theory

We now focus on a theoretic study on the l_1 -ball prior. Recall that the augmented prior $\pi_0(t, s, \mu)$ is a transform of $\pi_\beta(\beta)$, using $f : \mathbb{R}^p \rightarrow \{(t, s, \mu) \in \mathbb{R}^p \times \{1, -1\}^p \times \mathbb{R}_+ : \sum_{i=1}^p (t_i)_+ = r, t_i \geq -\mu/|C|\}$. We prove that f is invertible despite there is a dependency of μ on the ordering of $|\beta_i|$'s.,

Theorem 2. Consider a transform $\beta = g(t, s, \mu)$ with $C = \{i : t_i > 0\}$. If $|C| > 0$, let

$$\beta_i = s_i(t_i + \frac{\mu}{|C|}), \quad (5)$$

where its domain satisfies the following: $s_i \in \{-1, 1\}$; if $\sum_{i \in C} t_i = r$, then for $i \notin C$, $-\mu/|C| \leq t_i \leq 0$ and $\mu \geq 0$; if all $t_i \geq 0$ and $\sum t_i < r$, then $\mu = 0$. If $|C| = 0$, all $\beta_i = 0$. We have

$$f[g(t, s, \mu)] = (t, s, \mu), \quad g[f(\beta)] = \beta.$$

Remark 3. This means for any $\theta \in \mathbb{B}_r$, we can augment (t_i, s_i) 's for those $i \notin C$ and a $\mu \geq 0$, which forms a valid point in the pre-image of the l_1 -ball projection: $\beta : P_{\mathbb{B}_r}(\beta) = \theta$.

We can better understand the behavior of $\pi_0(\theta)$ if all the augmented latent variables $(t_i, s_i)_{i \notin C}$ and μ can be analytically marginalized. We have such a case, when β are assigned iid double-exponential density $\text{DE}(0, \lambda)$.

We now examine the case when temporarily treating r as given, which is meaningful for giving insights on how the radius influences the level of sparsity. In the first step now, we first treat r and λ as fixed and obtained the marginal form of $\pi_0(\theta \mid r)$ and $\text{pr}(|C| \mid r)$.

Theorem 3. If $\pi_\beta(\beta) = \prod_i (2\lambda)^{-1} \exp(-|\beta_i|/\lambda)$ with $\lambda > 0$, then for $\theta \in \mathbf{int} \mathbb{B}_r$, $\pi_0(\theta; r, \lambda) = \prod_i (2\lambda)^{-1} \exp(-|\theta_i|/\lambda) \mathbb{I}(\|\theta\|_1 < r)$, and for $\theta \in \mathbf{bd} \mathbb{B}_r$,

$$\pi_0(\theta \mid r) = \frac{(2\lambda)^{-|C|}}{\binom{p}{|C|}} \lambda \exp\left(-\frac{r}{\lambda}\right) \mathbb{I}(\|\theta\|_1 = r), \quad (6)$$

where $C = \{i \in [p] : \theta_i \neq 0\}$.

Further marginalizing over θ on $\{\theta : \|\theta\|_1 = r, \sum_{i=1}^p \mathbb{I}(\theta_i \neq 0) = j\}$, we can obtain a discrete prior distribution on the $|C|$.

Corollary 1. If $\pi_\beta(\beta) = \prod_i (2\lambda)^{-1} \exp(-|\beta_i|/\lambda)$ with $\lambda > 0$, then the marginal prior $\pi(|C|; r)$ follows a truncated Poisson distribution, with

$$pr(|C| = j \mid r) = \frac{(r/\lambda)^{j-1}}{(j-1)!} \exp\left(-\frac{r}{\lambda}\right), \quad (7)$$

for $j = 1, \dots, (p-1)$; and $pr(|C| = p \mid r) = 1 - \sum_{j=1}^{p-1} (r/\lambda)^{j-1}/(j-1)! \exp(-r/\lambda)$.

Remark 4. In the above, smaller r favors smaller $|C|$ (i.e., fewer $\theta_i \neq 0$).

We now focus on the likelihood under the regression settings and quantify the optimal convergence rate of the posterior. We will follow standard theoretic analysis [Castillo et al., 2015] by assuming y_i and θ_i are re-scaled by $1/\sigma$, so that $y_i \sim N(x_i' \theta, 1)$, while assuming there is an oracle $\theta^0 \in \mathbb{R}^p$, with $C_0 \neq 0$. In practice, since we do not know σ^2 we can assign a prior on $\sigma^2 \sim \text{Inverse-Gamma}(\gamma_{\sigma^2,1}, \gamma_{\sigma^2,2})$, and additionally let θ scale with σ .

To provide a much more straightforward result than the spike-and-slab prior, instead of resorting to $\tilde{\mu}$, we can choose a simple prior on r , $\pi_0(r) = \alpha^{-1} \exp(-r/\alpha)$ with α a parameter to determine. Multiplying it to (7) and integrating over r , and we obtain the marginal model selection probability under the $\pi_0(r)$:

$$pr(|C| = j; \lambda, \alpha) = \frac{\lambda/\alpha}{(1 + \lambda/\alpha)^j}, \quad (8)$$

for $j = 1, \dots, (p-1)$; and $pr(|C| = p; \lambda, \alpha) = 1 - \sum_{j=1}^{p-1} \lambda/\alpha (1 + \lambda/\alpha)^{-j} = (1 + \lambda/\alpha)^{-(p-1)}$. And

$$\pi_0(\theta; \lambda, \alpha) = \frac{(2\lambda)^{-|C|}}{\binom{p}{|C|}} \lambda/\alpha \exp\left[-(1/\lambda + 1/\alpha)^{-1} \|\theta\|_1\right], \quad (9)$$

for $|C| = 1, \dots, (p - 1)$. Recall that λ is the scale of $|\beta_i|$ before the thresholding, in order to induce a small $|C| \ll p$, we need a small radius by having its prior mean of radius $\alpha \ll \lambda$. We now formalize this intuition and present the convergence result.

Theorem 4. *If the data are generated from $y_i = X'_{i,:} \theta^0 + \epsilon_i$, $\epsilon_i \stackrel{iid}{\sim} N(0, 1)$, with (λ, α) chosen as $\lambda = b_1 p^{b_2} / \|X\|_{2,\infty}$, $\alpha = p^{b_3} / \|X\|_{2,\infty}$, $b_1 > 0$, $b_2 > b_3$, $b_3 \leq 1$, and $\|X\|_{2,\infty} := \max_j \sqrt{\sum_i X_{i,j}^2}$, with sufficiently large M , then as $n, p \rightarrow \infty$:*

- (Cardinality) For estimating the true cardinality c_0 ,

$$\sup_{\theta^0} \mathbb{E}_{\theta^0} \Pi \left(\theta : |C_\theta| > c_0 \left[1 + \frac{M}{b_2 - b_3} \left(1 + \frac{16}{\phi(C_0)^2} \frac{\lambda^*}{2\|X\|_{2,\infty} \sqrt{\log p}} \right) \right] \middle| Y \right) \rightarrow 0,$$

where $\lambda^* = \|X\|_{2,\infty} (b_1 p^{b_2} + p^{b_3}) / (b_1 p^{b_2} p^{b_3})$.

- (l_2 -recovery) The recovery of true θ^0 has

$$\sup_{\theta^0} \mathbb{E}_{\theta^0} \Pi \left(\theta : \|\theta - \theta^0\|_2 > \frac{M}{\psi(C_0)^2} \frac{\sqrt{c_0 \log p}}{\|X\|_{2,\infty} \phi(C_0)} \middle| Y \right) \rightarrow 0,$$

- (l_∞ -recovery) For every $\eta > 0$, any $d_0 < \eta^2 [1 + 2/(b_2 - b_3)]^{-1} / 8$, and c_n such that $c_n (b_1 p^{b_2} + p^{b_3}) \sqrt{\log p} / (b_1 p^{b_2} p^{b_3}) \rightarrow 0$, for the set $\mathcal{C}^* = \{C_0 : \phi(C_0) \geq \eta, \psi(C_0) \geq \eta, c_0 \leq c_n, c_0 \leq d_0 mc(X)^{-1}\}$, then the recovery of true θ^0 has

$$\sup_{\theta^0: C_0 \in \mathcal{C}^*} \mathbb{E}_{\theta^0} \Pi \left(\theta : \|\theta - \theta^0\|_\infty > M \frac{\sqrt{\log p}}{\|X\|_{2,\infty}} \middle| Y \right) \rightarrow 0.$$

In the above, $mc(X) = \max_{i \neq j} \frac{|X'_{:,i} X_{:,j}|}{\|X_{:,i}\|_2 \|X_{:,j}\|_2}$ is the mutual coherence, and $\phi(C), \psi(C)$ are the compatibility numbers for matrix X that we give the definitions in the appendix.

To illustrate the effects of the above theorem, we now compute the constants in several common scenarios. The first case is the normal mean problem: the model is based on $y_i = \theta_i + \epsilon_i$, with the goal to identify a few y_i that does not have the mean zero. This corresponds a design matrix $X = I_n$ and $n = p$, hence $\|X\|_{2,\infty} = 1$ and $\phi(C_0) = 1$. Therefore, the convergence rate for l_2 recovery is $\|\theta - \theta^0\|_2$ is $O[\sqrt{c_0 \log(n)}]$, which is the

optimal minimax rate [Castillo and van der Vaart, 2012] (if using stronger assumptions on c_0 , we expect the result to be extended to $O[\sqrt{c_0 \log(n/c_0)}]$). The second case is the sparse regression problem: the model is based on $y_i = X'_{i,\cdot} \theta + \epsilon_i$, with design matrix $X \in \mathbb{R}^{n \times p}$ and $n \ll p$. It is a common practice to standardize each column $X_{\cdot,j}$, so that $\sum_i X_{i,j}/n = 0$ and $\sum_i (X_{i,j} - \sum_i X_{i,j}/n)^2/(n-1) = 1$, therefore $\|X\|_{2,\infty} = \sqrt{n-1}$. For $c_0 \ll p$, we have an l_∞ recovery rate at $O(\log p / \sqrt{n})$; and the range of c_0 depends on the inverse of the maximal correlation of the columns of X , measured by $\text{mc}^{-1}(X)$. The third case is the change point detection problem, where $y_i = \sum_{t=1}^i \theta_t + \epsilon_i$ each i denoting a time point. The design matrix X is a lower-triangular matrix with $X_{i,j} = 1$ for $j \leq i$ and all other $X_{i,j} = 0$, which gives $\text{mc}(X) = \sqrt{(n-1)/n}$ and $\|X\|_{2,\infty} = \sqrt{n}$. For $c_0 \ll n$, we have an l_∞ recovery rate at $O(\log n / \sqrt{n})$.

4 Posterior Computation

The sampling of posterior (3) is amenable to the standard Markov chain Monte Carlo (MCMC). In linear regression settings, with $\pi_0(\beta)$ assigned to a double exponential prior, we have a simple posterior update using the Gibbs sampling. We will first show this algorithm.

Afterwards, we move to show a more general and automated approach for general models, exploiting the state-of-art optimization-based methods for posterior estimation [Dinh et al., 2016, Duan, 2019].

4.1 Gibbs Sampling Algorithm for Sparse Linear Problem

We first focus on likelihood,

$$L(y; X, \theta, \sigma^2) = (2\pi)^{-\frac{n}{2}} (\sigma^2)^{-\frac{n}{2}} \exp\left(-\frac{\|y - X\theta\|_2^2}{2\sigma^2}\right),$$

and independent prior for $\beta \sim \text{DE}(0, \lambda_i \sigma)$, with $\lambda_i \sim \text{Inverse-Gamma}(a, b)$, with $\tilde{\mu}$ chosen as the $(1-w)$ -quantile as described in Section 2.3, with using generalized double Pareto($a, b\sigma$), and a prior on $w \sim \text{Beta}(1, m)$. This leads to a prior on θ :

$$\pi_0(\theta) = c \exp\left(-\sum_{i \in C} \frac{\tilde{\mu}}{\lambda_i \sigma}\right) \left[\prod_{i \notin C} \frac{1}{2\lambda_i \sigma} \exp\left(-\frac{|\beta_i|}{\lambda_i \sigma}\right) \mathbb{I}(0 < |\beta_i| < \tilde{\mu}) \right] \left[\prod_{i \in C} \frac{1}{2\lambda_i \sigma} \exp\left(-\frac{|\theta_i|}{\lambda_i \sigma}\right) \right],$$

and we assign an improper non-informative prior $\pi(\sigma^2) \propto \sigma^{-2}$.

The Gibbs sampler iterates through the following steps.

1. We obtain $\beta_i = \text{sign}(\theta_i)(|\theta_i| + \tilde{\mu})$ for $i \in C$, and update the other β_i for $i \notin C$ via truncated exponential,

$$|\beta_i| \mid \tilde{\mu} \sim \text{Exp}(\lambda_i \sigma) \mathbb{I}(0 < |\beta_i| < \tilde{\mu}).$$

2. We update λ_i via

$$\lambda_i \mid \cdot \sim \text{Inverse-Gamma}(a + 1, b + |\beta_i|/\sigma).$$

3. We use the latent variable representation for double-exponential [Park and Casella, 2008]:

$$\frac{1}{2\lambda_i \sigma} \exp\left(-\frac{|\theta_i|}{\lambda_i \sigma}\right) = \int_0^\infty \frac{1}{\sqrt{2\pi} \sqrt{a_i \lambda_i^2 \sigma^2}} \exp\left(-\frac{\theta_i^2}{2a_i \lambda_i^2 \sigma^2}\right) \frac{1}{2} \exp\left(-\frac{a_i}{2}\right) da_i,$$

and a_i^{-1} for $i \in C$ follows an inverse-Gaussian $(\lambda_i \sigma / |\theta_i|, 1)$.

Using augmented $a_i^* = a_i$ if $i \in C$, and $a_i^* = 0$ if $i \notin C$. Given a_i^* , the conditional distribution of θ is a (potentially degenerated) Gaussian:

$$\theta \mid a^* \sim N(\Omega X' y, \sigma^2 \Omega),$$

where $\Omega = [X' X + \text{diag}(1/(a_i^* \lambda_i^2))]^{-1}$; if $a_i^* = 0$, both the mean and variance of θ_i become zero.

4. To enable blocked update, we follow George and McCulloch [1995] and use an approximation with a small $a^* = \epsilon$ if $i \notin C$. We first sample independently for $i = 1, \dots, p$,

$$\text{pr}(a_i^* = \epsilon) = \left\{ 1 + \frac{\exp[-\tilde{\mu}/(\sigma \lambda_i)]}{1 - \exp[-\tilde{\mu}/(\sigma \lambda_i)]} \frac{\sqrt{\epsilon}}{\sqrt{a_i}} \exp\left[-\frac{\theta_i^2}{2\lambda_i^2 \sigma^2} \left(\frac{1}{a_i} - \frac{1}{\epsilon}\right)\right] \exp\left(-\frac{a_i - \epsilon}{2}\right) \right\}^{-1},$$

and $\text{pr}(a_i^* = a_i) = 1 - \text{pr}(a_i^* = \epsilon)$; and to accommodate the term c that appears in the front of $\pi_0(\theta)$, we use these new a_i^* 's as proposal, and accept them with probability $\min(1, c^*/\tilde{c})$, where $c^* = \sum_{i=1}^p \mathbb{I}(a_i^* \neq \epsilon)$ based on the proposed a_i^* 's, and \tilde{c} based on the current a_i^* 's.

5. We can update σ^2 via the inverse-Gamma distribution

$$\pi(\sigma^2 \mid \cdot) \propto (\sigma^2)^{-(n+p)/2-1} \exp\left(-\frac{\|y - X\theta\|_2^2}{2\sigma^2} - \sum_{i=1}^p \frac{\beta_i^2}{2\lambda_i^2 \sigma^2 a_{\beta,i}}\right),$$

with $a_{\beta,i}^{-1} \sim \text{Inverse-Gaussian}(\lambda_i \sigma / |\beta_i|, 1)$.

6. Lastly, to update the parameter $w \in (0, 1)$ (hence the associated quantile $\tilde{\mu} = \tilde{\mu}_w$), we use the Metropolis-Hastings algorithm. From the current w , we generate a proposal $w^* \sim \text{Uniform}(w - \epsilon \vee 0, w + \epsilon \wedge 1)$, and evaluate:

$$h(w; w^*) = \exp\left(-\sum_{i \in C} \frac{\tilde{\mu}_w}{\lambda_i \sigma}\right) \prod_{i \notin C} \left[1 - \exp\left(-\sum_{i \in C} \frac{\tilde{\mu}_w}{\lambda_i \sigma}\right)\right] w^{m-1} \frac{1}{(w^* + \epsilon \wedge 1) - (w^* - \epsilon \vee 0)}$$

and accept w^* with probability $\min[1, h(w^*; w)/h(w; w^*)]$. To ensure this update does not directly change c , immediately after updating $\tilde{\mu}$, we update β_i for those $i \notin C$ so that those $|\beta_i| \leq \tilde{\mu}$.

4.2 Transport Monte Carlo for Sampling on l_1 -ball

We now move to more advanced models, such as the likelihood of non-linear model or/and correlated prior. As we obtain the l_1 -ball prior via a projection, the optimization-based posterior estimating methods, such as the Transport Monte Carlo [Duan, 2019] is convenient for such a purpose.

Recall that the target posterior distribution is:

$$\pi(\beta, \eta | y) = z^{-1} \pi_0(\eta) \pi_\beta(\beta) L[y; P_{\mathbb{B}_r}(\beta), \eta],$$

where z is the normalizing constant; and η involves other parameters including the radius r .

Transport Monte Carlo considers a joint distribution (also known as a ‘coupling’) of (η, β) with an auxiliary random variable $b \sim \pi(b)$ [b has the same number of elements as $(\eta, \beta) \in \mathbb{R}^{\tilde{p}}$].

$$\begin{aligned} \pi(\beta, \eta, b) &= \pi(\eta, \beta | y) \pi(b | \eta, \beta), \\ \pi(b | \eta, \beta) &= \sum_{k=1}^K w_k(\eta, \beta) \delta\{b - T_k^{-1}(\eta, \beta)\}, \end{aligned}$$

where T_k is an invertible transform with inverse T_k^{-1} , and δ is the Dirac function representing a point mass of b at $T_k^{-1}(\eta, \beta)$; (w_1, \dots, w_K) is a weight vector that can vary with (η, β) , and for any given (η, β) , $\sum_{k=1}^K w_k = 1$ and $w_k > 0$. That is, in this coupling each b is a random draw out of K candidate transforms from (η, β) ; as a result of invertibility, (η, β) is also a random draw out of K candidate transforms $T_k(b)$, which enables us to do rapid posterior sampling once $\pi(b), T_k$ and w_k are known. Calculation of the marginal gives us,

$$\pi(b) = \sum_{k=1}^K w_k \{T_k(b)\} \pi\{T_k(b) | y\} |\det \nabla T_k(b)|. \quad (10)$$

It was proved that, with K large enough, the above equality holds almost everywhere, for b following a uniform density $\pi(b) = 1$ for $b \in (0, 1)^{\tilde{p}}$.

In order to estimate the posterior, we first train the parameterized T_k and w_k , by sampling uniform b and minimizing the empirical Kullback-Leibler divergence between the two sides of (10). After the optimization converges, we can sample

$$b \stackrel{iid}{\sim} \pi(b), \quad (\beta, \eta) = T_k(b) \text{ with probability } v_k, \quad \theta = P_{\mathbb{B}_r}(\beta)$$

with $v_k \propto w_k \{T_k(b)\} \Pi \{T_k(b) \mid Y\} |\det \nabla T_k(b)|$.

This algorithm runs very efficiently: in all examples presented in the paper, we finish the posterior sampling within 5 minutes; Since the sampling of b is independent, the sampling of (θ, η) is independent as well. And we found in most cases, we need at most $K = 3$ to have the results indistinguishable from using larger K . The algorithmic details of Transport Monte Carlo (including choosing K and diagnostics of convergence) can be found in Duan [2019]. And we provide the relevant code in the supplementary materials.

5 Numeric Experiments

In this section, we use numeric experiments to illustrate the advantages of the l_1 -ball prior, and compare with the popular existing approaches, including both continuous shrinkage priors and the spike-and-slab prior.

5.1 Change Point Detection: Comparison with Continuous Shrinkage Prior

As motivated early, a key strength of the l_1 -ball prior is that it has exact zeros in the posterior. To show its necessity when applying the “ l_1 -tricks”, we first conduct a data analysis task of fitting a change point detection model, and compare the results with the horseshoe prior, as a popular continuous shrinkage prior.

The data are the cumulative sum of the daily return of Financial Times Stock Exchange 100 Index (FTSE 100 Index), which include $n = 300$ daily stock returns, collected during the trading period between the whole year of 1987 and early 1988.

The raw daily returns data are plotted in Figure 3, and we can see a few major change point events—for example, a sudden drop near day 200 and

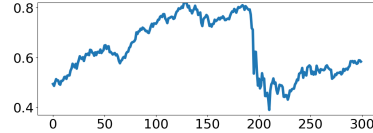
then a bounce back near day 250. We use the following model:

$$y_t = \sum_{i=1}^t \theta_i + \epsilon_t,$$

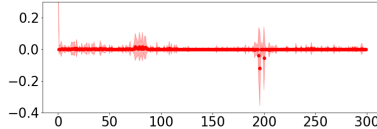
with $\epsilon \sim N(0, \sigma_\epsilon^2)$, $t \in \{1, \dots, 300\}$.

We can apply the “ l_1 -tricks” to make this a change point detection model: using a sparse prior on θ_i , if $\theta_t = \theta_{t+1} = \dots = \theta_{t+d} = 0$, then the mean curve is a flat line in $[t, t+d]$; changes occur only at the few points with $\theta_t \neq 0$.

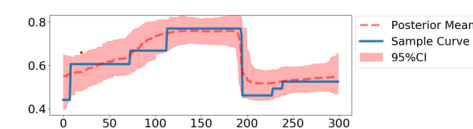
We use the l_1 -ball prior with $\beta_i \sim DE(0, \lambda_i)$, and $\tilde{\mu}$ as the $(1-w)$ -quantile as described in Section 2.4 with $b_w = p^{1.5} = 300^{1.5}$ [as a common strategy to allow sparsity to adapt to dimension Castillo et al. [2015]]. In the result shows a satisfactory step function with only a few changes (Figure 3). On the other hand, we test the continuous shrinkage prior using the horseshoe prior [Carvalho et al., 2010]. We use the half-Cauchy prior on the global parameter τ , and Jeffreys prior $\pi_0(\sigma_\epsilon^2) \propto \sigma_\epsilon^{-2}$ as the default prior. As shown in Panel (d) in Figure 3, although the continuous prior shrinks most of θ_t to near zero, the small values approximating zero accumulate over the time, causing the estimated function overfitted to small changes: not only the resulted function is far away from the desired step function, but the credible interval is very narrow—therefore, an ad-hoc thresholding cannot provide a good uncertainty quantification. To reduce the overfitting problem, we also test increasing σ_ϵ^2 to a fixed and larger value; however, this does not solve the problem, but creates sensitivity problem (the details are provided in the appendix).



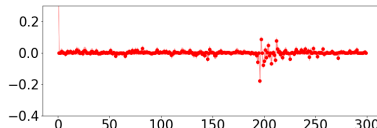
(a) The raw daily return data of FTSE 100.



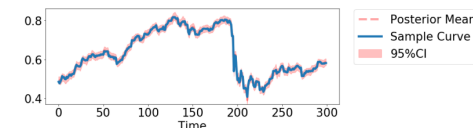
(b) The l_1 -ball posterior mean of θ with 95% point-wise credible intervals.



(c) The posterior sample curve of the l_1 -ball, with the posterior mean and 95% credible band.



(d) The horseshoe posterior mean of θ with 95% point-wise credible intervals.



(e) The posterior sample curve of horseshoe, with the posterior mean and 95% credible band.

Figure 3: Comparing the performances of applying l_1 -ball prior and continuous shrinkage prior in the change point detection model: the l_1 -ball produces a step function with a few steps corresponding to the major changes, while the continuous shrinkage prior (horseshoe in this case) fails to do so due to the too many small increments not exactly to zero.

5.2 Adaptive Shrinkage: Comparison with the Spike-and-Slab Prior

We now compare the performance of l_1 -ball prior with the spike-and-slab prior [Mitchell and Beauchamp, 1988, Castillo et al., 2015]. As mentioned in Section 2.3, the spike-and-slab prior can now be considered a special case of l_1 -ball prior, with β_i sharing a common scale parameter λ . Therefore, it is interesting to see if the new generalized model with individual scale λ_i can improve the performance.

To simulate the data, we use the sparse regression problem $x_i \sim N(0, I_p)$, $\epsilon_i \sim N(0, 1)$ and outcome $y_i = x_i' \theta^0 + \epsilon_i$, with $n = 200$, $p = 400$ and $c_0 = 5$. On the other hand, for the 5 non-zero θ_i^0 's, we use three different sets of values: (i) (100, 100, 100, 100, 100) as all signals away from 0, (ii) (1, 1, 1, 1, 1)

as all signals close to 0, and (iii) $(1, 1, 1, 1, 100)$ as a mix of both large and small signals [we consider $\theta_i^0 = 1$ as a small signal because it is in the same order as the noise variance $\text{var}(\epsilon_i) = 1$].

Figure 4 show a substantial difference between the two priors in settings (ii) and (iii). In the setting (ii), due the closeness between the signals and zero, the spike-and-slab prior has trouble identifying the differences—in panel (c) the common λ is an over-estimated scale for those $\theta_i = 0$ (showing excessive amount of variance), while underestimated scale for those $\theta_i^0 \neq 0$ (the posterior means for those non-zeros are much less than 1). This problem gets worse for the spike-and-slab prior in setting (iii) [panel (e)].

By comparison, the l_1 -ball prior with $\beta_i \sim \text{DE}(0, \lambda_i)$ shows a superior performance. We observe that the posterior samples for individual λ_i 's are indeed close to 0 where $\theta_i^0 = 0$, effectively making $\text{pr}(\theta_i = 0) \approx 1$. As a result, the variances at those points are very small [panel (d,f)]. At the same time, since each signal has its own scale, the posterior is less sensitive to overall strong shrinkage, giving a more accurate estimate [panel (d) vs. panel (c)].

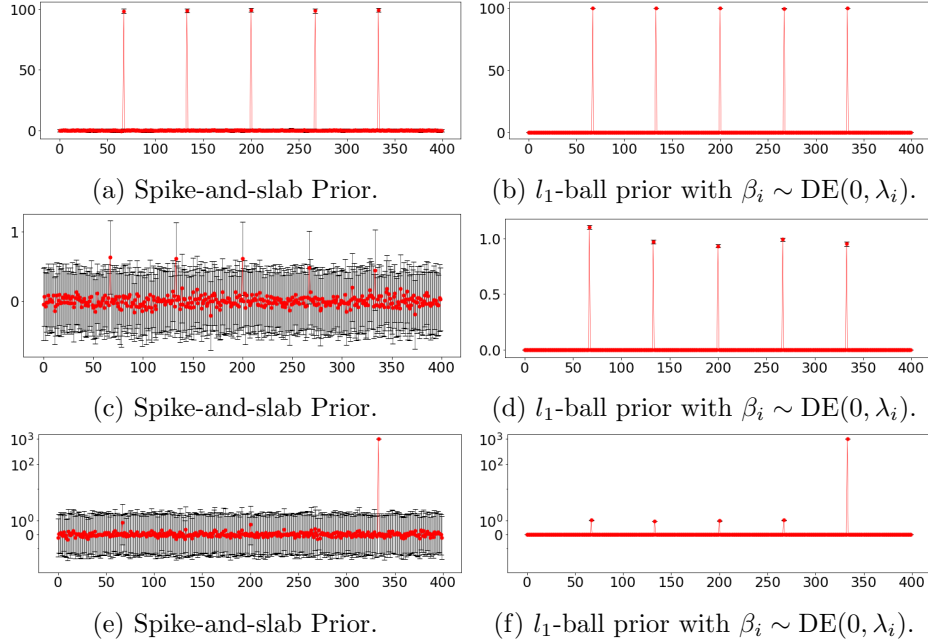


Figure 4: Comparing the performances of the spike-and-slab prior (the left panels) and the l_1 -ball prior with individual λ_i scale for each β_i (the right panels). When there are small signals [panels (c, e)] relatively close to zero, the spike-and-slab prior over-estimates their variances and show large error bars. The l_1 -ball prior can adapt to different levels of shrinkage [panel (d, f)]: those points that should be 0 has $\lambda_i \approx 0$ in the posterior, hence they have $\text{pr}(\theta_i = 0) = 1 - \exp(-\tilde{\mu}/\lambda_i) \approx 1$ and low variance, while the large signals can retain a large λ_i , hence is almost unaffected. The red dots are the posterior mean and the error bars are based on one standard deviation.

5.3 Sample Size and Sparsity Detection Limit

As discussed in the theory section, the recovery of θ^0 requires some conditions on the cardinality of the true parameter c_0 and the sample size n . We now use numerical simulations to empirically estimate the sparsity detection limits and required minimum sample size.

First, we focus on regression problems, with data simulated as described in the last section. We experiment with $p = 200, 300, 500$ and 800 , with n being a multiple of p and c_0 set to $25, 50, 75, 100, 150, 200$ times $\sqrt{1/\log p}$, as corresponding to different degrees of sparsity. To be consistent with theory result on regression, we benchmark the the sup-norm $\sup_i \|\hat{\theta}_i - \theta_i^0\|$ between

the posterior mean $\hat{\theta}$ and the oracle θ^0 . We plot the results in Figure 5, and make a few observations: (i) when $n \geq p$, all settings have low estimation errors close to zero; (ii) when $n < p$, we have good result roughly when $c_0 \leq 2\sqrt{n/\log p}$. This range is coherent with our theoretic analysis.

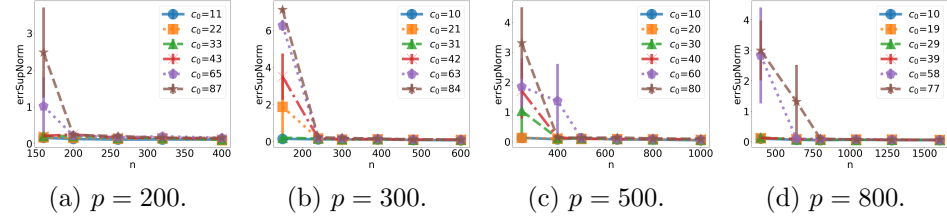


Figure 5: The simulation in sparse regression shows the l_1 -ball prior can correctly recover θ^0 in l_∞ norm when $c_0 \lesssim 2\sqrt{n/\log p}$.

Second, we experiment on change point detection. Note that in these settings we have square design matrix, i.e., $n = p$. We let p vary from 100, 200, 300, 500 and 800 and the sparsity level c_0 be a multiple of $\sqrt{p/\log p}$. Figure 6 shows that the l_1 -ball prior works well in change point detection $c_0 < 2\sqrt{p/\log p}$.

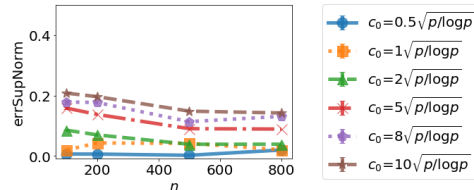


Figure 6: The l_1 -ball prior can recover θ^0 in l_∞ norm in change point detection.

5.4 Further Benchmark Results

In addition, we compare the performance of the l_1 -ball prior with the Bayesian lasso and horseshoe priors, over a range of different p , n and c_0 . For conciseness, we provide the results in the appendix.

6 Data Application: Clustering of Electroencephalogram Time Series using Mixture of Linear Trends

We now use the l_1 -ball prior in a more advanced model motivated by a scientific application. The task is to analyze the electroencephalogram (EEG) data obtained from a neuroscience study. The volunteers are asked to wear an EEG cap on the scalp that records the electric activity of their brains, while performing a cognitive task related to memory function. There are $M = 128$ electrode channels, each producing one time series containing $T = 130$ time points, reflecting the neuron activity near the electrode. Our goal is to address two scientific questions: is there an inherent group structure among those 128 channel positions? what is the common trend in each group?

We use the following model based on an infinite mixture of temporal functions:

$$\begin{aligned} y_t^{(m)} &\sim N[f^{(m)}(t) + \eta_m, \sigma_m^2] \\ [f^{(m)}, \sigma_m^2] &\sim \sum_{k=1}^{\infty} w_k \delta_{f_*^{(k)}, \sigma_{k*}^2}(\cdot) \\ w_k &= v_k \prod_{k' < k} (1 - v_k), \quad v_k \sim \text{Beta}(1, 0.1), \end{aligned}$$

for $m = 1, \dots, M$; where $\eta_m \sim N(0, 100)$ is a random intercept accommodating the overall shift for each time series; $\delta_a(x)$ denotes a point mass at a ; w_k is the mixture weight, following a stick-breaking construction. In this model, each mixture component is the vector output of $f^{(m)}(t)$, a piecewise linear function over $t = 1, \dots, T$, and the noise variance $\sigma_k^2 \sim \text{Inverse-Gamma}(2.5, 2.5)$.

One can immediately see the main modeling complexity is to parametrize a piecewise function for $f^{(m)}(t)$. This is where we use the l_1 -tricks, by over-parametrizing

$$f_*^{(k)}(t) = \mu^{(k)}(t),$$

and penalizing the second finite difference of

$$2\mu^{(k)}(t) - \mu^{(k)}(t-1) - \mu^{(k)}(t+1).$$

Note that if the above is exactly zero, then the three points $f_*^{(k)}(t-1), f_*^{(k)}(t), f_*^{(k)}(t+1)$ are on a single line.

Following Kim et al. [2009], we reparameterize $\vec{\mu}^{(k)} = X'\theta^{(k)}$, with X a lower-triangular matrix, with the first column $X_{i,1} = 1$, while $X_{i,j} = i - j + 1$ for $1 < j \leq i$, and all other $X_{i,j} = 0$.

Figure 7 shows the trend estimation of the three clusters. The l_1 -ball prior captures the piece-wise linear trend in time series along with the uncertainty quantification. We see the distinct patterns of three groups: group 3 has the least fluctuation during the whole time periods, suggesting that there are not much activities in the corresponding brain regions. On the other hand, groups 1 and 2 display multiple peaks and turning points in the series. One may notice that group 1 and 2 differ a lot around time point 100: groups 2 is flat while groups 1 experiences a severe drop.

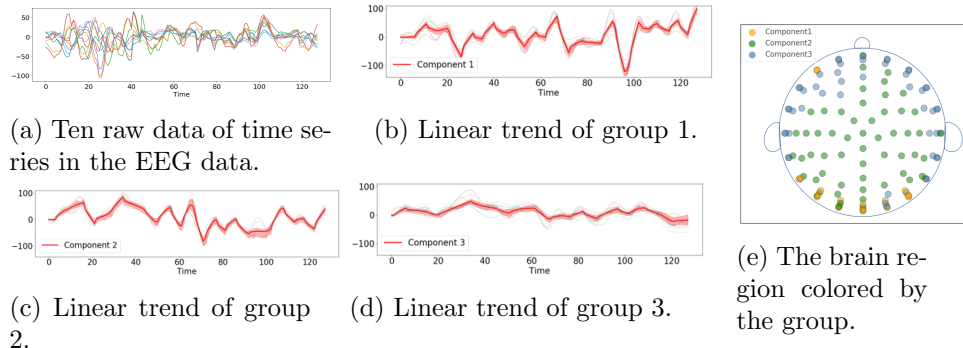


Figure 7: Linear trend clustering of 128 EEG time series. The red line with shadow is the fitted piece-wise linear line and its 95% credible band, and the transparent colored curves are the observed time series in corresponding cluster.

7 Discussion

In this paper, we propose a new sparsity-induced prior by projecting a continuous prior onto the l_1 -ball. There are several interesting extensions that can be pursued: (i) we can follow the same methodology presented, and consider a more complicated projection. For example, for a Bayesian extension of the convex clustering (Tan and Witten [2015], using $y_i \sim N(\theta_i, \sigma^2 I_p)$), we can have a high dimensional continuous prior for $\beta \in \mathbb{R}^{n(n-1)/2}$, then project it to the low-dimensional space $\theta = \arg \min_{\mu \in \mathcal{C}} \|\text{vec}(\|\mu_i - \mu_j\|_2)_{(i < j)} - \beta\|_2$, where $\mathcal{C} = \{\mu \in \mathbb{R}^{n \times p} : \sum_{i < j} (\|\mu_i - \mu_j\|_2) \leq r\}$, making most of $\theta_i - \theta_j = 0$ and leading to clustering. (ii) To directly extend the l_1 -prior we have illustrated, one can consider a more flexible structure on the distribution of β , such as the correlation structure on β as suggested. Alternatively, one can use other family of continuous distribution to impose some specific prior information—for example, a Gaussian mixture on β with some components

far away outside the l_1 -ball, hence creating even stronger shrinkage.

References

Artin Armagan, David B Dunson, and Jaeyong Lee. Generalized double pareto shrinkage. *Statistica Sinica*, 23(1):119, 2013.

Ray Bai and Malay Ghosh. On the beta prime prior for scale parameters in high-dimensional bayesian regression models. *Statistica Sinica*, 2019.

Anirban Bhattacharya, Debdeep Pati, Natesh S Pillai, and David B Dunson. Dirichlet–laplace priors for optimal shrinkage. *Journal of the American Statistical Association*, 110(512):1479–1490, 2015.

Peter Bühlmann and Sara Van De Geer. *Statistics for High-dimensional Data: Methods, Theory and Applications*. Springer Science & Business Media, 2011.

Carlos M Carvalho, Nicholas G Polson, and James G Scott. The horseshoe estimator for sparse signals. *Biometrika*, 97(2):465–480, 2010.

Ismaël Castillo and Aad van der Vaart. Needles and straw in a haystack: Posterior concentration for possibly sparse sequences. *The Annals of Statistics*, 40(4):2069–2101, 2012.

Ismaël Castillo, Johannes Schmidt-Hieber, and Aad Van der Vaart. Bayesian linear regression with sparse priors. *The Annals of Statistics*, 43(5):1986–2018, 2015.

Scott Shaobing Chen, David L Donoho, and Michael A Saunders. Atomic decomposition by basis pursuit. *SIAM Review*, 43(1):129–159, 2001.

Laurent Dinh, Jascha Sohl-Dickstein, and Samy Bengio. Density estimation using real nvp. *arXiv preprint arXiv:1605.08803*, 2016.

Leo L Duan. Transport monte carlo. *arXiv preprint arXiv:1907.10448*, 2019.

John Duchi, Shai Shalev-Shwartz, Yoram Singer, and Tushar Chandra. Efficient projections onto the l_1 -ball for learning in high dimensions. In *Proceedings of the 25th International Conference on Machine Learning*, pages 272–279, 2008.

Bradley Efron, Trevor Hastie, Iain Johnstone, and Robert Tibshirani. Least angle regression. *The Annals of Statistics*, 32(2):407–499, 2004.

Jianqing Fan, Han Liu, Yang Ning, and Hui Zou. High dimensional semi-parametric latent graphical model for mixed data. *Journal of the Royal Statistical Society: Series B (Statistical Methodology)*, 79(2):405–421, 2017.

Edward I George and Robert E McCulloch. Stochastic search variable selection. *Markov chain Monte Carlo in Practice*, 68:203–214, 1995.

Edouard Grave, Guillaume R Obozinski, and Francis R Bach. Trace lasso: a trace norm regularization for correlated designs. In *Advances in Neural Information Processing Systems*, pages 2187–2195, 2011.

Hemant Ishwaran and J Sunil Rao. Spike and slab variable selection: Frequentist and bayesian strategies. *The Annals of Statistics*, 33(2):730–773, 2005.

Seung-Jean Kim, Kwangmoo Koh, Stephen Boyd, and Dimitry Gorinevsky. l_1 trend filtering. *SIAM Review*, 51(2):339–360, 2009.

Fred B Lempers. *Posterior Probabilities of Alternative Linear Models*. Rotterdam University Press, 1971.

Fredrik Lindsten, Henrik Ohlsson, and Lennart Ljung. Clustering using sum-of-norms regularization: With application to particle filter output computation. In *2011 IEEE Statistical Signal Processing Workshop (SSP)*, pages 201–204. IEEE, 2011.

Nicolai Meinshausen and Peter Bühlmann. High-dimensional graphs and variable selection with the lasso. *The Annals of Statistics*, 34(3):1436–1462, 2006.

Toby J Mitchell and John J Beauchamp. Bayesian variable selection in linear regression. *Journal of the American Statistical Association*, 83(404):1023–1032, 1988.

Trevor Park and George Casella. The bayesian lasso. *Journal of the American Statistical Association*, 103(482):681–686, 2008.

volume=113 number=521 pages=431–444 year=2018 publisher=Taylor & Francis Ročková, Veronika and George, Edward I, journal=Journal of the American Statistical Association. The spike-and-slab lasso.

Ali Shojaie and George Michailidis. Penalized likelihood methods for estimation of sparse high-dimensional directed acyclic graphs. *Biometrika*, 97(3):519–538, 2010.

Kean Ming Tan and Daniela Witten. Statistical properties of convex clustering. *Electronic Journal of Statistics*, 9(2):2324, 2015.

Martin A Tanner and Wing Hung Wong. The calculation of posterior distributions by data augmentation. *Journal of the American Statistical Association*, 82(398):528–540, 1987.

Robert Tibshirani. Regression shrinkage and selection via the lasso. *Journal of the Royal Statistical Society: Series B (Methodological)*, 58(1):267–288, 1996.

Robert Tibshirani, Michael Saunders, Saharon Rosset, Ji Zhu, and Keith Knight. Sparsity and smoothness via the fused lasso. *Journal of the Royal Statistical Society: Series B (Statistical Methodology)*, 67(1):91–108, 2005.

Roman Vershynin. *High-dimensional Probability: An Introduction with Applications in Data Science*, volume 47. Cambridge University Press, 2018.

Ming Yuan and Yi Lin. Model selection and estimation in regression with grouped variables. *Journal of the Royal Statistical Society: Series B (Statistical Methodology)*, 68(1):49–67, 2006.

Teng Zhang and Hui Zou. Sparse precision matrix estimation via lasso penalized d-trace loss. *Biometrika*, 101(1):103–120, 2014.

Hui Zou and Trevor Hastie. Regularization and variable selection via the elastic net. *Journal of the Royal Statistical Society: Series B (Statistical Methodology)*, 67(2):301–320, 2005.

Hui Zou, Trevor Hastie, and Robert Tibshirani. Sparse principal component analysis. *Journal of Computational and Graphical Statistics*, 15(2):265–286, 2006.

Appendix

Proof of Theorem 1

Proof. Since permutation of indices does not affect $|J|$, without loss of generality, we assume $\sum_{i=1}^c |\theta_i| = r$ and $|\theta_i| > 0$ for $i = 1, \dots, c$.

Now f^{-1} is a mapping from $(\theta_1, \dots, \theta_{c-1}, t_{c+1}, \dots, t_p, \mu)$ to $(\beta_1, \dots, \beta_{c-1}, \beta_{c+1}, \dots, \beta_p, \beta_c)$, where $\beta_c = s_c(r - \sum_{i=1}^{c-1} |\theta_i| + \mu/c)$. The Jacobian matrix J is

$\frac{\partial}{\partial \theta_1}$	β_1	\dots	β_{c-1}	β_{c+1}	\dots	β_p	β_c
	1	\dots	0	0	\dots	0	$-s_1 s_c$
\vdots	\vdots	\ddots	\vdots	\vdots	\vdots	\vdots	\vdots
$\frac{\partial \theta_{c-1}}{\partial t_{c+1}}$	0	\dots	1	0	\vdots	0	$-s_{c-1} s_c$
	0		0	s_{c+1}	0	0	0
\vdots	\vdots	\vdots	\vdots	\vdots	\ddots	\vdots	\vdots
$\frac{\partial t_p}{\partial \mu}$	0	\dots	0	0	\dots	s_p	0
	s_1/c	\dots	s_{c-1}/c	s_{c+1}/c	\dots	s_p/c	s_c/c

Split the matrix into four blocks, with $A = J_{1:(p-1), 1:(p-1)}$, $B = J_{p, 1:(p-1)}$, $C = J_{1:(p-1), p}$ and $D = s_c/c$. We know

$$\begin{aligned}
|J| &= |D - BA^{-1}C||A| \\
&= |s_c/c + \sum_{i=1}^{c-1} s_i^2 s_c/c| \times 1 \\
&= |s_c| \\
&= 1.
\end{aligned}$$

□

Proof of Theorem 2

Proof. With β_i 's re-ordered $|\beta_{(1)}| \geq \dots \geq |\beta_{(p)}|$, we will prove $|\beta_{(j)}| > (\sum_{i=1}^j |\beta_{(i)}| - r)/j$ for all $j \leq |C|$ and $|\beta_{(j)}| < (\sum_{i=1}^j |\beta_{(i)}| - r)/j$ for $j > |C|$. This is equivalent to comparing $(j-1)|\beta_{(j)}| - (\sum_{i=1}^{j-1} |\beta_{(i)}| - r)$ against 0.

When $j \leq |C|$,

$$\begin{aligned}
&(j-1)|\beta_{(j)}| - (\sum_{i=1}^{j-1} |\beta_{(i)}| - r) \\
&= (j-1)(|\theta_{(j)}| + \frac{\mu}{|C|}) - \{ \sum_{i=1}^{j-1} (|\theta_{(i)}| + \frac{\mu}{|C|}) - r \} \\
&= (j-1)|\theta_{(j)}| - (\sum_{i=1}^{j-1} |\theta_{(i)}| - r) \\
&> 0,
\end{aligned}$$

since $\sum_{i=1}^{j-1} |\theta_{(i)}| < r$ for $j \leq |C|$.
When $j > |C| + 1$,

$$\begin{aligned}
& (j-1)|\beta_{(j)}| - \left(\sum_{i=1}^{j-1} |\beta_{(i)}| - r \right) \\
&= (j-1)\left(t_{(j)} + \frac{\mu}{|C|}\right) - \left\{ \sum_{i=1}^{|C|} \left(|\theta_{(i)}| + \frac{\mu}{|C|}\right) + \sum_{i=|C|+1}^{j-1} \left(t_{(i)} + \frac{\mu}{|C|}\right) - r \right\} \\
&= (j-1)t_{(j)} - \left\{ \sum_{i=1}^{|C|} |\theta_{(i)}| + \sum_{i=|C|+1}^{j-1} t_{(i)} - r \right\} \\
&\stackrel{(a)}{=} (j-1)t_{(j)} - \sum_{i=|C|+1}^{j-1} t_{(i)} \\
&\stackrel{(b)}{<} (j-1-|C|)t_{(j)} - \sum_{i=|C|+1}^{j-1} t_{(i)} \\
&= \sum_{i=|C|+1}^{j-1} (t_{(j)} - t_{(i)}) \\
&\stackrel{(c)}{\leq} 0,
\end{aligned}$$

where (a) is due to $\sum_{i=1}^{|C|} |\theta_{(i)}| = r$, (b) due to $t_{(j)} < 0$ and (c) due to $|\beta_{(j)}| - \mu/|C| \leq |\beta_{(i)}| - \mu/|C|$ for $j > i$.

When $j = |C| + 1$, $(j-1)|\beta_{(j)}| - \left(\sum_{i=1}^{j-1} |\beta_{(i)}| - r \right) = |C|t_{(j)} < 0$.

Therefore, we have $c = |C|$, and it can be verified that in (1)

$$\mu_c = \sum_{i=1}^{|C|} \left(|\theta_{(i)}| + \frac{\mu}{|C|} \right) - r = \mu.$$

□

Proof of Theorem 3

Proof. For ease of notation, we denote $\vec{t}_{\bar{C}} := t_{\sigma_1}, \dots, t_{\sigma_{p-|C|}}$

$$\begin{aligned}
\pi_0(\theta) &= \sum_{\substack{s_{\sigma_1}, \dots, s_{\sigma_{p-|C|}} \\ \in \{-1, 1\}^{p-|C|}}} \int_0^\infty \int_{(-\mu/|C|, 0)^{p-|C|}} \pi_\beta\{g(t, s, \mu)\} d\vec{t}_{\bar{C}} d\mu \\
&= 2^{p-|C|} (2\lambda)^{-p} \int_0^\infty \int_{(-\mu/|C|, 0)^{p-|C|}} \prod_{i \in C} \left\{ e^{-\frac{|\theta_i| + \mu/|C|}{\lambda}} \right\} \prod_{i \in \bar{C}} \left\{ e^{-\frac{t_i + \mu/|C|}{\lambda}} \right\} d\vec{t}_{\bar{C}} d\mu \\
&= 2^{p-|C|} (2\lambda)^{-p} \prod_{i \in C} \left\{ \exp\left(-\frac{|\theta_i|}{\lambda}\right) \right\} \int_0^\infty e^{-\frac{p\mu}{\lambda|C|}} \int_{(-\mu/|C|, 0)^{p-|C|}} \prod_{i \in \bar{C}} e^{-\frac{t_i}{\lambda}} d\vec{t}_{\bar{C}} d\mu \\
&= 2^{p-|C|} (2\lambda)^{-p} \exp\left(-\frac{r}{\lambda}\right) \cdot \lambda^{p-|C|} \int_0^\infty e^{-\frac{p\mu}{\lambda|C|}} \left(e^{\frac{\mu}{\lambda|C|}} - 1 \right)^{p-|C|} d\mu.
\end{aligned}$$

Let $u = e^{-\frac{\mu}{\lambda|C|}}$, then $du = -(\lambda|C|)^{-1} e^{-\frac{\mu}{\lambda|C|}} d\mu$, we have

$$\int_0^\infty e^{-\frac{p\mu}{\lambda|C|}} \left(e^{\frac{\mu}{\lambda|C|}} - 1 \right)^{p-|C|} d\mu = \lambda|C| \int_0^1 u^{|C|-1} (1-u)^{p-|C|} du = \lambda \frac{\Gamma(|C|+1)\Gamma(p-|C|+1)}{\Gamma(p+1)}.$$

Combining the results,

$$\pi_0(\theta) = \frac{(2\lambda)^{-|C|}}{\binom{p}{|C|}} \lambda \exp\left(-\frac{r}{\lambda}\right)$$

□

Proof of Corollary 1

Proof. We first focus on when $\|\theta\|_1 < r$, since under which, $|C| < p$ happens with probability zero, therefore,

$$\begin{aligned}
\text{pr}(|C| = p, \|\theta\|_1 < r) &= \int_{\mathbb{R}^p} \prod_i (2\lambda)^{-1} \exp(-|\theta_i|/\lambda) \mathbb{I}(\|\theta\|_1 < r) d\theta \\
&= \int_{\mathbb{R}_+^p} \prod_i (\lambda)^{-1} \exp(-x_i/\lambda) \mathbb{I}(\sum x_i < r) dx \\
&\stackrel{(a)}{=} \int_0^r \frac{1}{\Gamma(p)\lambda^p} y^{p-1} \exp(-y/\lambda) dy \\
&\stackrel{(b)}{=} 1 - \sum_{j=0}^{p-1} \frac{1}{j!} \left(\frac{r}{\lambda}\right)^j \exp(-r/\lambda),
\end{aligned}$$

where (a) uses the fact that sum of p iid $\text{Exp}(\lambda)$'s is a $\text{Gamma}(p, \lambda)$, and (b) uses the CDF formula as p is an integer.

When $\|\theta\|_1 = r$, and $|C| = j$, denote the non-zero indices by $\{i_1, \dots, i_j\}$, note that $x = (|\theta_{i_1}|/r, \dots, |\theta_{i_j}|/r)$ is on a probability simplex with dimension $(j-1)$, Δ^{j-1} , hence we can use Dirichlet distribution integral $\int_{\Delta^{j-1}} 1 dx = 1/\Gamma(j)$. We have

$$\begin{aligned} \text{pr}(|C| = j, \|\theta\|_1 = r) &= \frac{(2\lambda)^{-j}}{\binom{p}{j}} \lambda \exp\left(-\frac{r}{\lambda}\right) 2^j \binom{p}{j} r^{j-1} / \Gamma(j) \\ &= \left(\frac{r}{\lambda}\right)^{j-1} \exp\left(-\frac{r}{\lambda}\right) / (j-1)!, \end{aligned}$$

for $j = 1, \dots, p$. Combining the above gives the result. \square

Proof of Theorem 4

Proof. The compatibility numbers are

$$\begin{aligned} \phi(C) &= \inf_{\beta} \left\{ \frac{\|X\beta\|_2 |C|^{1/2}}{\|X\|_{2,\infty} \|\beta_C\|_1} : \|\beta_{[p] \setminus C}\|_1 \leq 7 \|\beta_C\|_1, \beta_C \neq 0 \right\}, \\ \psi(C_0) &= \tilde{\phi} \left[\left(2 + \frac{3}{a+b} + \frac{33}{\phi(C_0)^2} \frac{\lambda^*}{2\|X\|_{2,\infty} \sqrt{\log p}} \right) c_0 \right], \\ \tilde{\phi}(c) &:= \inf \left\{ \frac{\|X\theta\|_2}{\|X\| \|\theta\|_2} : 0 \neq |C_\theta| \leq c \right\}. \end{aligned}$$

Our results are based on the early work of Castillo et al. [2015], Theorems 1 and 2: For a constant λ^* and a discrete distribution $g(c)$ supported on $\{0, \dots, p\}$, when

1. $\|X\|_{2,\infty}/p \leq \lambda^* \leq 4\|X\|_{2,\infty}\sqrt{\log p}$,
2. There exist constants $a_1, a_2, a_3, a_4 > 0$ with (2.2) $a_1 p^{-a_3} \leq \frac{g(c)}{g(c-1)} \leq a_2 p^{-a_4}$ for $c = 2, \dots, p$.

Then for a prior kernel of the form

$$\pi_0(\theta; \lambda^*, g) = g(|C|) \frac{1}{\binom{p}{|C|}} \left(\frac{\lambda^*}{2}\right)^{|C|} \exp(-\lambda^* \|\theta\|_1),$$

with $g(|C| = j) = \text{pr}(|C| = j)$, would enjoy the results in the theorem. We now check these two conditions, and compute the associated constants.

Using the chosen λ and α , we have

$$\lambda^* = \frac{\lambda + \alpha}{\lambda\alpha} = \|X\|_{2,\infty} \frac{b_1 p^{b_2} + p^{b_3}}{b_1 p^{b_2} p^{b_3}},$$

Since $b_3 \leq 1$, we have $\lambda^* \geq \|X\|_{2,\infty}/p^{b_3} \geq \|X\|_{2,\infty}/p$. Since $b_2 > b_3$, for p large enough, $b_1 p^{b_2} > p^{b_3}$, hence $\|X\|_{2,\infty}(b_1 p^{b_2} + p^{b_3})/(b_1 p^{b_2} p^{b_3}) \leq 2/p^{b_3} \|X\|_{2,\infty} \leq 4\|X\|_{2,\infty}\sqrt{\log p}$.

On the other hand, When $c = 1, \dots, p-1$.

$$\frac{g(c)}{g(c-1)} = (1 + \lambda/\alpha)^{-1} = \frac{1}{1 + b_1 p^{b_2 - b_3}}.$$

Clearly, $g(c)/g(c-1) \leq 1/(b_1 p^{b_2 - b_3})$, satisfying $a_2 = 1/b_1$ and $a_4 = b_2 - b_3$. For p large enough $b_1 p^{b_2 - b_3} > 1$, we have $g(c)/g(c-1) \geq 1/(2b_1 p^{b_2 - b_3})$, satisfying $a_1 = 1/(2b_1)$ and $a_3 = b_2 - b_3$. When $c = p$, $g(c)/g(c-1) = \alpha/\lambda = 1/(b_1 p^{b_2 - b_3})$, hence also satisfying the above results. Therefore, we apply $a_4 = b_2 - b_3$ in the two theorems of Castillo et al. [2015], and arrive at our results. \square

Additional Simulation of Change Point Detection using Continuous Prior

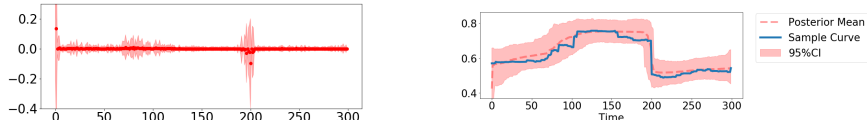


Figure 8: Change point detection using the horseshoe prior with an increased noise variance $\sigma_\epsilon^2 = 0.05$: the model still overfits to the small changes, yet fails to capture some important change events, such as the bounce-back near day 250.

Additional Benchmark Results

We now benchmark using the canonical regression settings for two Bayesian continuous priors: the horseshoe [Carvalho et al., 2010] and the Bayesian lasso [Park and Casella, 2008], implemented through R packages `monomvn` and `horseshoe` in regression problem. Specifically, in the model $y_i = x_i' \theta + \epsilon_i$, with $X \in \mathbb{R}^{n \times p}$ and ϵ_i from $N(0, 1)$. We fix $n = 200$ and consider $p = 200$ and 500 . For each p , we let the true cardinality to be $c_0 = 5, 10$ and 20 .

For each experiment setting, the n rows of the design matrix $X \in \mathbb{R}^{n \times p}$ are independently drawn from $N(0, I_p)$. We generate the true θ^0 according to the level of sparsity, where the non-zero entries are drawn from $N(5, 1)$. For the global shrinkage parameter τ in the horseshoe, we assign a half-Cauchy prior $\mathcal{C}^+(0, 1)$.

We use the posterior mean $\hat{\theta}$ to compute the 2-norm error, $\|\hat{\theta} - \theta^0\|_2$. We also compute the estimated cardinality \hat{c} through averaging the number of non-zero entries of each posterior sample. Since the continuous shrinkage priors assign zero mass to exact sparse vectors, we use an approximate measure of cardinality $\hat{c} = \#\{\theta_i : |\theta_i| > \delta\}$ and we choose $\delta = 0.1\sigma$ in this study.

As shown in Figure 9, Panel (a) and (b), l_1 -ball enjoys the least l_2 norm in both cases. Between the two continuous priors, the horseshoe is more competitive especially when the model is sparse. Panel (c) and (d) shows that the l_1 -ball gives a good estimation on the cardinality.

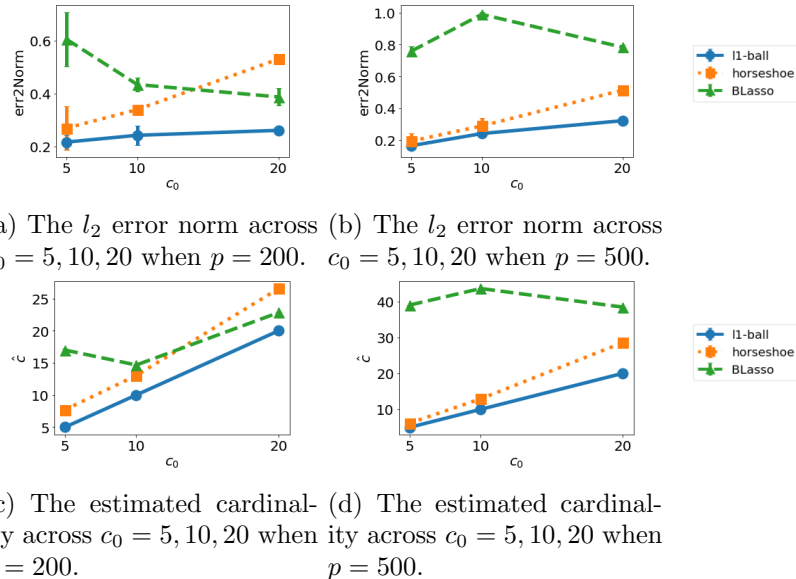


Figure 9: Comparing the l_1 -ball, the horseshoe and the Bayesian lasso in different dimensionality and sparsity levels. The l_1 -ball enjoys the smallest error norm and the closest estimation for c_0 .